Study on Fluid Flow and Heat Transfer Characteristics in a Flat Heat Pipe

Kyu Hyung Do †, Sung Jin Kim*

평판형 히트 파이프 내의 유체 유동 및 열전달 특성에 관한 연구

도규형 † · 김성진*

Key Words : Flat heat pipe (평판형 히트 파이프), Thin film evaporation (박막 증발), The augmented Young-Laplace equation (증대된 영-라플라스 방정식)

Abstract

In this study, a mathematical model for a thermal analysis of a flat heat pipe with a grooved wick structure is presented. The effects of the liquid-vapor interfacial shear stress, the contact angle, and the amount of liquid charge have been included in the proposed model. In particular, the axial variations of the wall temperature and the evaporation/condensation rates are considered by solving the one-dimensional conduction and the augmented Young-Laplace equations, respectively. In order to verify the model, the results obtained from the model are compared to existing experimental data.

Nomenclature

A_r	aspect ratio of the groove
D_h	hydraulic diameter, m
fRe	Poiseuille number
h	heat transfer coefficient, W/m^{2}K
h_{fg}	specific heat of vaporization, J/kg
P	perimeter, m
δ	liquid film thickness, m
Γ	mass flow rate, kg/s
γ	contact angle

1. Introduction

Miniature and conventional heat pipes with axial grooves can be successfully used in electronic components cooling systems [1]. As the power density of critical electronic components is increased, the need for a heat pipe with a higher thermal performance is increased. Jacobs and Harnett [2] predicted that chip heat fluxes in mainframe computers will exceed 100 W/cm^2 by the year 2000. Cao et al. [3] noted that heat fluxes generated by metal oxide semiconductor controlled thyristors are already in the range of 100 W/cm^2 to 300 W/cm^2.

Several researchers have experimentally shown that flat heat pipes with axial capillary grooves could be applied in the cooling of high heat flux electronic devices [3-5]. Plesch et al. [4] performed a limited investigation of copper-water heat pipes with overall dimensions of 7 mm×2 mm×120 mm with a series of 80 axial rectangular capillary grooves machined on the inner surface. Power was uniformly applied to both wide evaporator walls over a surface area of 2 cm^2 and removed at the condenser by a constant temperature (42^{o}C) coolant flow. A maximum heat flux was found of 35 W/cm^2 in the horizontal orientation and 60 W/cm^2 in the vertical orientation where the condenser was above the evaporator. Cao et al. [3] tested an 82-mm long copper-water flat heat pipe with overall dimensions similar to the Plesch et al. heat pipe. The capillary structure consisted of a series of axial rectangular grooves along the entire inner perimeter of the heat pipe and the vapor passage cross-sectional area was approximately 4 mm^2. A maximum heat flux obtained was restricted by the capillary limit and reached 18.3 W/cm^2 with a positive inclination angle of 20^o. Hopkins et al. [5] performed experimental and theoretical analysis for copper-water flat heat pipes with overall dimensions of 13.41 mm×8.92 mm×120 mm with a series of 62 axial rectangular capillary grooves machined on the inner surface. Maximum heat fluxes with a uniform heat load applied to both sides were found to be 92.8 W/cm^2 in the horizontal orientation and 141.8 W/cm^2 in the vertical orientation, respectively. However, the theoretical results

† Korea Advanced Institute of Science and Technology
E-mail : doggu@kaist.ac.kr
TEL : (042)869-3083 FAX : (042)869-8207
* Korea Advanced Institute of Science and Technology

for the maximum heat flux in the horizontal orientation underestimated the experimental results by as much as 35 percent.

Many researchers have suggested analytical models which are simple one-dimensional models based on the differential form of the Laplace-Young equation to characterize the thermal performance of micro/miniature heat pipes with various cross sectional and groove shape [6-9]. However, these models employ many simplifying assumptions to facilitate the analysis. First, evaporation and condensation are assumed to occur uniformly in the axial direction. Secondly, it is also assumed that evaporation occurs in the only evaporator section and condensation occurs in the only condenser section inside the heat pipe. Finally, the wall temperature is either assumed to be constant or excluded in the analysis. These assumptions may lead to significant errors for predicting the thermal performance of the heat pipe. Therefore, the axial variations of the wall temperature and the evaporation and condensation rates should be taken into account to precisely predict the fluid flow and heat transfer phenomena in micro/miniature heat pipes.

The purpose of the present study is to develop a mathematical model for precisely predicting fluid flow and heat transfer phenomena in a flat heat pipe with a grooved wick structure. The effects of the liquid-vapor interfacial shear stress, the contact angle, and the amount of liquid charge are included in the proposed model. In particular, the axial variations of the wall temperature and the evaporation and condensation rates are considered by solving the one-dimensional conduction equation for the wall and the augmented Young-Laplace equation, respectively. In order to verify the model, the results obtained from the model are compared to existing experimental data. By using the suggested model, the effect of the amount of liquid charge on the thermal performance of the flat heat pipe is also examined.

2. Mathematical Model

2.1 Governing equations

The system being studied herein is a flat heat pipe with rectangular grooves, as shown in Fig. 1. The governing equations are derived under the following assumptions: i) one-dimensional steady incompressible flow along the length of the heat pipe; ii) one-dimensional temperature variation for the wall of the heat pipe along the axial direction; iii) negligible convection in the liquid and vapor. In order to establish the governing equations the heat pipe is divided into a series of small control volumes (*CV*) of length, *dx*. The continuity equations for the liquid and vapor regions are expressed as follows:

$$V_{v,i}P_{v,i} - A_v\frac{du_v}{dx} = 0, \quad \text{in the vapor region} \tag{1}$$

$$-V_{l,i}P_{l,i} - A_l\frac{du_l}{dx} = 0, \quad \text{in the liquid region} \tag{2}$$

$$\rho_v V_{v,i}P_{v,i} = N\rho_l V_{l,i}P_{l,i} \tag{3}$$

$V_{v,i}$, $P_{v,i}$, A_v, u_v, $V_{l,i}$, $P_{l,i}$, A_l, ,u_l denote the averaged interfacial velocity and perimeter at the liquid-vapor interface, cross-sectional area, and the axial velocity for the vapor region and the averaged interfacial velocity and perimeter at the liquid-vapor interface, cross-sectional area, and the axial velocity for the liquid region, respectively. From the mass continuity across the interface, as shown in Eq. (3), the averaged interfacial velocity for the liquid phase can be expressed as

$$V_{l,i} = \frac{\rho_v P_{v,i}}{N\rho_l P_{l,i}}V_{v,i} \tag{4}$$

The averaged interfacial velocity, $V_{v,i}$ is obtained by solving the augmented Young-Laplace equation. Details are explained in the next section.

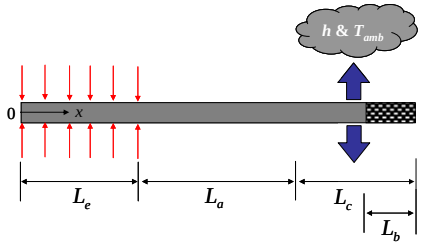

(a) Overall dimension

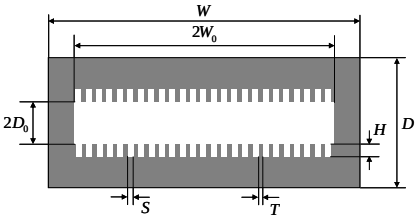

(b) Cross-sectional dimension

Fig.1 Schematic diagram of a flat heat pipe

The conservation of axial momentum equation for an incompressible vapor flow is written as

$$-2\rho_v A_v u_v\frac{du_v}{dx} - \left(\tau_{v,w}P_{v,w} + \tau_{v,i}P_{v,i}\right) - A_v\frac{dp_v}{dx} = 0 \tag{5}$$

where $\tau_{v,w}$ and $\tau_{v,i}$ are the wall and interfacial shear stresses in the vapor region, respectively. Since the present model is one-dimensional, information about these shear stresses is unknown. To compute these shear stresses, the vapor flow is assumed to be similar to fully developed duct flow. For a rectangular vapor channel configuration the wall and interfacial shear stresses can be defined using the following equation [10].

$$\tau_{v,w} = \tau_{v,i} = \frac{24\mu_v u_v}{\pi^2 W_0}\frac{\displaystyle\sum_{n=1}^{\infty}\frac{(-1)^{n-1}}{(2n-1)^2}\tanh\left[\frac{(2n-1)\pi D_0}{2W_0}\right]}{\left[1-\frac{192}{\pi^5}\left(\frac{W_0}{D_0}\right)\displaystyle\sum_{n=1}^{\infty}\frac{1}{(2n-1)^5}\tanh\left[\frac{(2n-1)\pi D_0}{2W_0}\right]\right]} \tag{6}$$

Equation (7) represents the conservation of momentum equation for the liquid flow in a groove with cross-section area, A_l.

$$\frac{dp_l}{dx} = -\frac{2\mu_l u_l}{D_{h,l}^2}(f\,\mathrm{Re})_l \tag{7}$$

For the liquid flow the inertial effects are negligible in comparison to those due to viscous losses [8]. The values of $(f\mathrm{Re})_l$ can be taken from the correlation suggested by Schneider and DeVos [11].

$$(f\,\mathrm{Re})_l = (f\,\mathrm{Re})_{l0}\left\{1+\frac{D_{h,l}\tau_{v,i}}{\mu_l u_l}\frac{1}{3(2Ar)^2}\left[1-1.971\exp(-\pi Ar)\right]\right\} \quad (8)$$

where $(f\mathrm{Re})_{l0}$ corresponds to the case of no liquid-vapor interaction.

$$(f\,\mathrm{Re})_{l0} = \frac{8(2Ar)^2}{(1+2Ar)^2\left[\frac{1}{3}-\frac{64}{\pi^5(2Ar)}\tanh(\pi Ar)\right]},\quad Ar=\frac{H}{S}$$

In the present study, the axial variation of the wall temperature is taken into account. In most previous models, the wall temperature is either assumed to be constant or excluded in the analysis. This assumption may lead to significant errors for predicting the thermal performance of the heat pipe when the working fluid of the heat pie is overcharged or the wall thickness is relatively large. The conservation of energy equation including the heat pipe wall conduction is given as

$$k_s A_s \frac{d^2T_w}{dx^2} - \rho_v V_{v,i} P_{v,i} h_{fg} + q''_w P_w = 0 \quad (9)$$

where k_s, A_s, T_w, P_w, and q''_w are the thermal conductivity, the cross-sectional area, and temperature of the heat pipe wall, the outer wall perimeter of the heat pipe, and the heat flux at the wall, respectively. The heat flux profiles at the wall can be expressed as follows:

$$q''_w(x) = \begin{cases} Q_{in}/P_w L_e, & 0 \le x \le L_e \\ 0, & L_e < x < L_e + L_a \\ -h\left[T_w(x) - T_{amb.}\right], & L_e + L_a \le x \le L_t \end{cases} \quad (10)$$

h denotes the local heat transfer coefficient between the external surface of the heat pipe and the ambient in the condenser section. In addition, the present model considers the heat transfer in the liquid block region. In the liquid block region, condensation dose not occur because the vapor region and grooves are filled with the liquid. Kim et al. [9] mentioned that the liquid block acts as a thermal barrier for the condensation heat transfer due to its lower thermal conductivity. However, heat is still transferred by conduction from the liquid to the wall of the heat pipe. The heat rate per unit length by conduction can be obtained by solving the 2D conduction problem with geometry and boundary conditions as shown in Fig.2.

$$Q'_b = \frac{2N}{\pi} k_f \left(T_v - T_w(x)\right) \sum_{n=1}^{\infty} \frac{1+(-1)^{n+1}}{n} \frac{-\cos(n\pi)}{\tanh(n\pi H/S)} \quad (11)$$

Therefore, the conservation of energy equation is divided into two regions and Eq. (9) can be rewritten as

$$\begin{cases} k_s A_s \dfrac{d^2T_w}{dx^2} - \rho_v V_{v,i} P_{v,i} h_{fg} + q''_w P_w = 0, & 0 \le x \le L_t - L_b \\ k_s A_s \dfrac{d^2T_w}{dx^2} + Q'_b + q''_w P_w = 0, & L_t - L_b < x \le L_t \end{cases} \quad (12)$$

The interfacial radius of the meniscus curvature is related to the pressure difference between the liquid and vapor by the Laplace-Young equation, which, in differential form, is

$$\frac{dp_v}{dx} - \frac{dp_l}{dx} = -\frac{\sigma}{r_c^2}\frac{dr_c}{dx} \quad (13)$$

Equations (1), (2), (5), (7), (12), and (13) constitute a set of five first-order and one second-order nonlinear coupled ordinary differential equations in 7 unknowns: u_v, u_l, p_v, p_l, T_w, dT_w/dx, and r_c. The boundary conditions used at the beginning of the evaporator section are

$$r_c\big|_{x=0} = r_{c,\min} \quad (14)$$

$$u_l\big|_{x=0} = u_v\big|_{x=0} = 0 \quad (15)$$

$$p_v\big|_{x=0} = p_{sat}(T_v),\quad p_l\big|_{x=0} = p_{sat}(T_v) - \sigma/r_{c,\min} \quad (16)$$

$$T_w\big|_{x=0} = T_{w,e},\quad \left.\frac{dT_w}{dx}\right|_{x=0} = 0 \quad (17)$$

Here p_v is taken to be the saturation pressure of the vapor at temperature, T_v. If a heat pipe is transport heat, a minimum capillary radius should be formed at the beginning of the evaporator section and a maximum capillary radius at the point where the liquid block starts in the condenser section [5]. It is assumed that the maximum capillary radius equals the hydraulic radius of the vapor region at $x = L_t - L_b$ [8], which is regarded as the convergence criterion of the capillary radius. Equations (1), (2), (5), (7), (12), and (13) with boundary conditions are solved numerically using the fourth-order Runge-Kutta method.

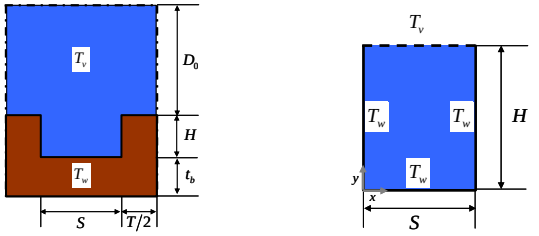

(a) Entire cross section (b) Computational domain

Fig. 2 Schematic cross section of the liquid block region

2.2 Determination of the evaporation/condensation rate

Most previous models have used the assumptions that evaporation and condensation occur uniformly in the axial direction, evaporation occurs in the only evaporator section, and condensation occurs in the only condenser section [6-9]. However, these assumptions are no longer valid when the wall temperature varies along the axial direction or evaporation or condensation occurs inside the heat pipe in the adiabatic section. Vadakkan et al. [12] showed that there is no adiabatic section inside the heat pipe from their numerical result. The evaporation and condensation rates are obtained by solving the augmented Young-Laplace equation in the present study.

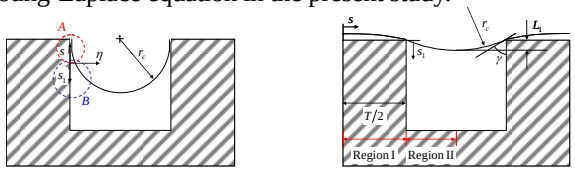

(a) Evaporator (b) Condenser

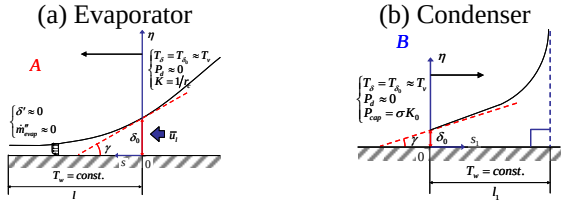

Fig. 3 Cross sections of liquid-filled groove

2.2.1 Evaporation region

In this section, an evaporating film on a heat-loaded surface is considered, as shown in Fig. 3(a). The

extended meniscus formed on the heated wall is characterized by three regions: i) the adsorbed film region, where this film cannot be evaporated due to the high adhesion forces; ii) the evaporating thin film region, so called micro-region, where the major part of evaporation occurs; iii) the meniscus region, where the adhesion forces are negligible and the meniscus curvature radius is constant. In the evaporating thin film region, a one-dimensional laminar boundary layer approximation for the transverse liquid flow is used (see Fig. 3). The mass flow rate is given as

$$\Gamma = \rho_l \int_0^{\delta} \bar{u}_l d\eta = -\frac{\delta^3}{3\nu_l}\frac{dp_l}{ds} \tag{18}$$

where ν_l is the kinematic viscosity. Following Wayner et al. [13, 14], the evaporative mass flux is modeled as a function of the temperature and pressure jumps at the interface according to the expression

$$\dot{m}''_{evap} = a\left(T_\delta - T_v\right) + b\left(p_l - p_v\right) \tag{19}$$

where T_δ is the temperature of the liquid-vapor interface and T_v is the temperature of the vapor. The liquid-vapor interfacial temperature and the wall temperature are related by the one-dimensional conduction heat transfer equation as follows:

$$k_l \frac{T_w - T_\delta}{\delta} = \dot{m}''_{evap} h_{fg} \tag{20}$$

Following Moosman and Homsy [15], Eq. (19) and Eq. (20) may be combined to eliminate T_δ in favor of T_w:

$$\dot{m}''_{evap} = \left(1 + \frac{a h_{fg}}{k_l}\delta\right)^{-1} \left[a\left(T_w - T_v\right) + b\left(p_l - p_v\right)\right] \tag{21}$$

The continuity equation for the evaporating liquid layer is

$$\frac{d\Gamma}{ds} = -\dot{m}''_{evap} \tag{22}$$

Substituting Eqs. (18) and (21) into Eq. (22), the coupled differential equation can be written as

$$-\frac{1}{3\nu_l}\frac{d}{ds}\left(\delta^3 \frac{dp_l}{ds}\right) = \left(1 + \frac{a h_{fg}}{k_l}\delta\right)^{-1} \left[a\left(T_w - T_v\right) + b\left(p_l - p_v\right)\right] \tag{23}$$

In the evaporating thin film region, the pressure difference between the vapor and liquid at the liquid-vapor interface is due to both the capillary and disjoining pressure, and is expressed using the augmented Young-Laplace equation [13]:

$$p_v - p_l = p_d + \sigma \frac{d^2\delta}{ds^2}\left[1 + \left(\frac{d\delta}{ds}\right)^2\right]^{-3/2} \tag{24}$$

where the first term on the right-hand side is known as the disjoining pressure and the second term on the right-hand side is the capillary pressure which is the product of interfacial curvature, K and surface tension coefficient, σ. The vapor pressure is assumed to be constant along the s-axis. The disjoining pressure is expressed as

$$p_d = A/\delta^3 \tag{25}$$

where A is the dispersion constant and δ is film thickness. In the present study, A is taken from the theoretical results of Wayner [16] and 5.942×10^{-21} J. Differential Eqs. (23) and (24) must be solved for four variables: δ, δ', $(p_v - p_l)$, and $(p_v - p_l)'$ in the interval from $s = 0$ to $s = l$ with their respective boundary conditions:

$$\delta\big|_{s=0} = \delta_0,\ \delta'\big|_{s=0} = -\tan\gamma \tag{26}$$

$$\left(p_v - p_l\right)\big|_{s=0} = \sigma K_0,\ \left(p_v - p_l\right)'\Big|_{s=0} = 0 \tag{27}$$

where K_0 is the curvature in the meniscus region and γ is the contact angle. The value of δ_0 is found from Eq. (24) when the disjoining pressure is negligibly small compared with the capillary pressure in the meniscus region ($p_d \approx 10^{-5} p_{c0}$). Although the initial-value problem, Eqs. (23) and (24) with B.C.s Eq. (25) and (26), is completely determined, its solutions must satisfy one more condition:

$$\dot{m}''_{evap}\big|_{s=l} = 0 \tag{28}$$

Since the length of the evaporating thin film region is not specified. As a result of this problem, the evaporative mass flux profile in the evaporating thin film region can be obtained, as shown in Eq. (21).

In the meniscus region, the liquid-vapor interfacial temperature is almost the same as the vapor temperature and the disjoining pressure is negligible. The governing equation and boundary conditions are

$$\frac{d^2\delta}{ds_1^2} = K_0\left[1 + \left(\frac{d\delta}{ds_1}\right)^2\right]^{3/2} \tag{29}$$

$$\delta\big|_{s_1=0} = \delta_0,\ \left.\frac{d\delta}{ds_1}\right|_{s_1=0} = \tan\gamma,\ \left.\frac{d\delta}{ds_1}\right|_{s_1=l_1} \approx \tan\frac{\pi}{2} \tag{30}$$

The evaporative mass flux in the meniscus region is

$$\dot{m}''_{evap} = \frac{k_l}{h_{fg}}\frac{T_w - T_v}{\delta} \tag{31}$$

Therefore, the averaged interfacial velocity in the evaporation region can be expressed as

$$V_{v,i} = \frac{2N}{\rho_v P_{v,i}}\left[\int_0^l \dot{m}''_{evap} ds + \int_0^{l_1} \dot{m}''_{evap} ds_1\right] \tag{32}$$

2.2.2 Condensation region

At the condensation region, the condensing film is divided into two regions, as shown in Fig. 3(b): i) a thin film region at the fin top; ii) a meniscus region of the constant curvature. Analyzing heat transfer in the thin film region, simplifying assumptions are employed. One is that the film thickness variation along the s-axis is weak. The other is that the disjoining pressure gradient along the film flow can be neglected in comparison to that of the capillary pressure. From these assumptions, the governing equation and boundary conditions for the film thickness at the fin top are given as

$$\frac{\sigma}{3\nu_l}\frac{d}{ds}\left(\delta^3\frac{d^3\delta}{ds^3}\right) = -\left(1 + \frac{a h_{fg}}{k_l}\delta\right)^{-1}\left[a\left(T_w - T_v\right) + b\left(p_l - p_v\right)\right] \tag{33}$$

$$\left.\frac{d\delta}{ds}\right|_{s=0} = \left.\frac{d^3\delta}{ds^3}\right|_{s=0} = 0,\ \left.\frac{d^2\delta}{ds^2}\right|_{s=T/2} = \frac{1}{r_c},\ \left.\frac{d\delta}{ds}\right|_{s=T/2} = -\tan\left(\frac{\pi}{2} - \gamma\right) \tag{34}$$

The boundary value problem, Eq. (32) with B.C.s Eq. (34), is solved approximately by introducing the following polynomial function for the film thickness.

$$\delta(s) = C_0 + \sum_{n=1}^{4} C_n \left(s - T/2\right)^n \tag{35}$$

From the boundary conditions Eq. (35) the values of the coefficients are

$$C_1 = -\tan(\pi/2-\gamma),\ C_2 = 1/2r_c,\ C_3 = 4C_4L_1,\ C_4 = -\frac{C_1 - 2C_2L_1}{8L_1^3} \quad (36)$$

In order to determine the coefficient, C_0, the condition that the total mass flow rate must be equal to the total amount of fluid condensed in the region $0 \le s \le T/2$ is used. Integrating Eq. (33) and then substituting Eq. (35) into Eq. (37), C_0 can be obtained.

$$\frac{\sigma}{3v_l}\left[\delta^3\frac{d^3\delta}{ds^3}\bigg|_{s=T/2} - \delta^3\frac{d^3\delta}{ds^3}\bigg|_{s=0}\right] = -\int_0^{T/2}\frac{a(T_w - T_v) + b(p_l - p_v)}{1 + \frac{ah_{fg}}{k_l}\delta}ds \quad (37)$$

By using Eq. (35), the condensation mass flux profiles in the thin film region can be obtained as

$$\dot{m}''_{cond} = \left(1 + \frac{ah_{fg}}{k_l}\delta\right)^{-1}\left[a(T_w - T_v) + b(p_l - p_v)\right] \quad (38)$$

Heat transfer problem for the meniscus region in the condensation region is very similar to that in the evaporation region. The condensation mass flux in the meniscus region is written as

$$\dot{m}''_{cond} = \frac{k_l}{h_{fg}}\frac{T_w - T_v}{\delta} \quad (39)$$

Therefore, the averaged interfacial velocity in the condensation region can be expressed as

$$V_{v,i} = \frac{2N}{\rho_v P_{v,i}}\left[\int_0^{T/2}\dot{m}''_{cond}ds + \int_0^{L_1}\dot{m}''_{cond}ds_1\right] \quad (40)$$

2.3 Solution procedure

When the heat pipe with a rectangular grooved wick structure is to transport its maximum amount of heat, a minimum capillary radius at the beginning of the evaporator section is defined as the following equation.

$$r_{c,\min} = \frac{S}{2\cos\gamma} \quad (41)$$

However, if the heat pipe is to transport a certain amount of heat, which is smaller than the maximum heat transport rate, it is expected from physical insight that the capillary radius at the beginning of the evaporator section is larger than that written in Eq. (41). Therefore, when the input heat load is given, the complete solutions for Eqs. (1), (2), (5), (7), (12), and (13) can be obtained by determining the minimum capillary radius which satisfies the convergence criterion. When the minimum capillary radius is given as Eq. (41), the complete solutions for the governing equations can be obtained by determining the maximum input heat load which satisfies the convergence criterion.

3. Results and Discussion

In order to validate the present model, the wall temperature profiles and the maximum heat transport rate obtained from the model are compared with the experimental results of Hopkins et al. [5]. Geometric parameters of the experimental copper-water heat pipe and other relevant specifications of the experiment are summarized in Table 1.

Table 1 Specification of the flat heat pipe

W (mm)	13.41	N (ea.)	62
D (mm)	8.92	L_e (mm)	15.6
W_0 (mm)	4.875	L (mm)	70.0
D_0 (mm)	0.61	L_c (mm)	34.4
H (mm)	0.42	Q_{in} (W)	0 – 120
S (mm)	0.2	T_v (^{o}C)	60 – 95
T (mm)	0.1	Liquid Fill (ml)	0.84 (40%)

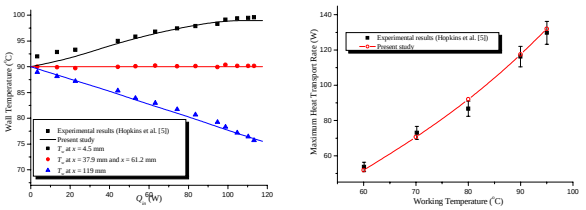

(a) Wall temperature (b) Q_{max}

Fig. 4 Comparison of the results obtained from the model with experimental results of Hopkins et al. [5]

Figure 4 shows the comparison between the results from the model and experimental data. The results from the present model are in close agreement with the experimental data for the wall temperatures and the maximum heat transport rate with maximum errors of 2% and 5%, respectively. Figure 5 illustrates the axial wall temperature profile for Q_{in} = 100 W and T_v = 90 ^{o}C. According to the results from the present model, the liquid block length of the flat heat pipe used in experiments makes up about 58 percent of the condenser section. A substantial overcharging of the working fluid causes a large temperature drop in the liquid block region, as shown in Fig. 5(a). The heat rate per unit length profile along the axial direction is represented in Fig. 5(b). As we expected, evaporation and condensation rates are not uniform but varied along the axial direction. In the adiabatic section, heat transfer by evaporation or condensation takes place inside the heat pipe. Therefore, the assumption that evaporation occurs in the only evaporator section and condensation occurs in the only condenser section is no longer valid in this case

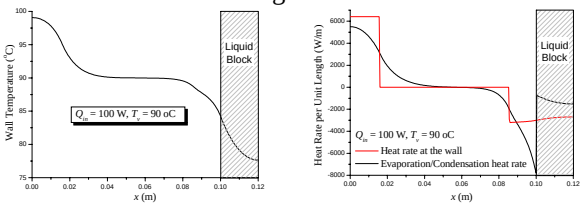

(a) Wall temperature (b) Heat rate per unit length

Fig. 5 Wall temperature and Heat rate profiles

3.1 Effect of the amount of liquid charge

As mentioned before, the increase of the liquid block length results in a large temperature drop. To examine the effect of the amount of liquid charge on the thermal performance of the flat heat pipe, the filling ratio, which is defined as the ratio of the liquid volume to the empty volume inside the heat pipe, is varied from 0.29 to 0.475. When the filling ratio is 0.29, the liquid block length is zero and the liquid block length is equal to the condenser section length for the filling ratio of 0.475. For evaluating the thermal performance of the heat pipe, the

maximum heat transport rate and the thermal resistance as the objective functions are chosen. The thermal resistance, R, is defined here as the overall end cap to end cap temperature drop divided by the input heat load.

$$R = \left(T_{w,e} - T_{w,c}\right) / Q_{in} \quad (42)$$

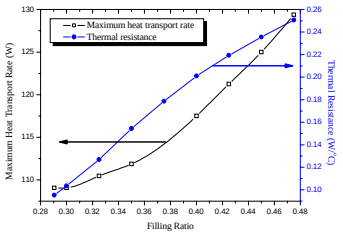

Fig. 6 Effect of the filling ratio on Q_{max} and R

Figure 6 illustrates the effect of the filling ratio on the maximum heat transport rate, Q_{max} and the thermal resistance, R. As the filling ratio increases, Q_{max} slightly increases. This is because flow resistance decreases due to the decrement of the effective length of the heat pipe. The thermal resistance increases with increasing the filling ratio. When the filling ratio is 0.475 ($L_b = L_c$) Q_{max} is enhanced up to about 19% compared with that for the filling ratio of 0.29 (L_b = 0). On the other hand, the thermal resistance is increased by about 160% compared with that for the filling ratio of 0.29. This means that the larger the filling ratio, the worse the thermal performance of the heat pipe. Hence, the thermal performance of the heat pipe is maximized when the filling ratio is 0.29 (L_b = 0).

4. Conclusion

A mathematical model for precisely predicting the thermal performance of a flat heat pipe with a grooved wick structure is developed.. The results obtained from the proposed model are in close agreement with existing experimental data for the wall temperatures and the maximum heat transport rate. From the validated model, it is found that the assumptions employed in most previous may lead to significant errors for predicting the thermal performance of the heat pipe. Finally, the effect of the amount of liquid charge on the thermal performance of the flat heat pipe is examined. As the amount of liquid charge increases, Q_{max} slightly increases due to the decrement of the effective heat pipe length, while thermal resistance remarkably increases with increasing the amount of liquid charge. The thermal performance of the heat pipe is maximized when the liquid block length is zero.

Acknowledgements

This work was supported by the Korea Science & Engineering Foundation through the NRL Program (grant 2006-02147).

References

1. A. Faghri, Heat Pipe Science and Technology, *Taylor & Fancis* (1995).
2. H. R. Jacobs and J. P. Hartnett, Thermal Engineering: Emerging Technologies and Critical Phenomena, *Workshop Report*, NSF Grant No. CTS-91-04006, 139-176 (1991).
3. Y. Cao, J. E. Beam, and B. Donovan, Air-Cooling System for Metal Oxide Semiconductor Controlled Thyristors Employing Miniature Heat Pipes, *J. Thermophysics Heat Transfer*, 10 (3), 484-489 (1996).
4. D. Plesch, W. Bier, D. Seidel, and K. Schubert, Miniature Heat Pipes for Heat Removal From Microelectronic Circuits, *Proc. ASME Annual Meeting*, Atlanta, GA (1991).
5. R. Hopkins, A. Faghri, and D. Khrustalev, Flat Miniature Heat Pipes with Micro Capillary Grooves, *J. Heat Transfer* 121, 102-109 (1999).
6. B. R. Babin, G. P. Peterson, and D. Wu, Steady-State Modeling and Testing of a Micro Heat Pipe, *J. Heat Transfer* 112, 595-601 (1990).
7. J. P. Longtin, B. Badran, and F. M. Gerner, A One-Dimensional Model of a Micro Heat Pipe During Steady-State Operation, *J. Heat Transfer* 116, 709-715 (1994).
8. D. Khrustalev and A. Faghri, Thermal Analysis of a Micro Heat Pipe, *J. Heat Transfer* 116, 189-198 (1994).
9. S. J. Kim, J. K. Seo, and K. H. Do, Analytical and Experimental Investigation on the Operational Characteristics and the Thermal Optimization of a Miniature Heat Pipe with a Grooved Wick Structure, *Int. J. Heat Mass Transfer* 42, 3405-3418 (2003).
10. F. M. White, Viscous Fluid Flow, *McGraw-Hill* (1991).
11. G. E. Schneider and R. DeVos, Nondimensional Analysis for the Heat Transport Capability of Axially-Grooved Heat Pipes Including Liquid/Vapor Interaction, *AIAA Paper*, 80-0214 (1980).
12. U. Vadakkan, J. Y. Murthy, and S. V. Garimella, Transient Analysis of Flat Heat Pipes, *ASME Summer Heat Transfer Conference*, LasVegas, Nevada (2003).
13. P. C. Jr. Wayner, K. Y. Kao, and L. V. LaCroix, The Interline Heat Transfer Coefficient of an Evaporating Wetting Film, *Int. J. Heat Mass Transfer* 19, 487-492 (1976).
14. P. C. Jr. Wayner, The Effect of Interfacial Mass Transport on Flow in Thin Liquid Films, *Colloids Surfaces* 52, 71-84 (1991).
15. S. Moosman and S. M. Homsy, Evaporating Menisci of Wetting Fluids, *J. Colloid Interface Sci.* 73, 212-223 (1980).
16. P. C. Jr. Wayner, The Effect of the London-Van Der Waals Dispersion Force on Interline Heat Transfer, *J. Heat Transfer* 100, 155-159 (1978).